Available online at www.sciencedirect.com

ScienceDirect

Photonics and Nanostructures – Fundamentals and Applications 12 (2014) 350–359

PHOTONICS AND NANOSTRUCTURES
Fundamentals and Applications

www.elsevier.com/locate/photonics

Radiation from a short vertical dipole in a metal-backed rod array

Yang Li [a,*], Mário G. Silveirinha [b]

[a] Department of Electrical and Computer Engineering, Baylor University, Waco, TX 76798, United States
[b] Departamento de Engenharia Electrotécnica, Instituto de Telecomunicacões, Universidade de Coimbra, 3030 Coimbra, Portugal

Received 20 February 2014; received in revised form 21 April 2014; accepted 5 May 2014
Available online 3 July 2014

Abstract

Based on an effective medium approach, we investigate the problem of radiation of a short vertical electric dipole embedded in a metal-backed dielectric rod array. We obtain the radiated electromagnetic field in the form of a Sommerfeld integral, and calculate the near and far electric fields for both lossless and lossy rod arrays. The characteristic equation for the guided modes is derived and solved. The guided modes are found to be slow waves and their propagation constants and modal distributions are extracted. All theoretical results are compared with full-wave simulations.

Keywords: Dielectric rod array; Effective medium theory; Radiation; Propagation

1. Introduction

A dielectric rod array – understood as a 2-D periodic structure formed by either infinite-length or finite-length cylindrical dielectric rods – has long been of interest because of its unique electromagnetic characteristics. It was used as a dielectric waveguide element in a phased array [1], as well as a photonic bandgap (PBG) structure [2]. More recently, arrays of negative permittivity rods have also received great attention due to their unusual potentials in manipulating the near-field in the nanoscale [3–8], in enhancing light-matter interactions [9–17], and in controlling the radiative heat transfer [18].

In a different research direction, a dielectric rod array may be used to represent a simple scaled forest model. For example, the dielectric constant of water at microwave frequencies (77-j10 at 2.5 GHz) is close to that of typical pine trees at HF/VHF frequencies (50-j15 at 50 MHz [19]). Based on this observation, a periodic array consisting of water-filled straws was introduced to represent a 1:50 scaled forest model in both measurements [20] and full-wave numerical simulations [21]. While modeling vegetation media as a periodic dielectric array is evidently a very rough approximation in areas where the vegetation is dominated by grass, this approach can provide relevant physical insights in other scenarios (e.g. areas with tall tree trunks), and we expect that for some kinds of aligned forest it can capture the main physical mechanisms of the electromagnetic wave propagation, in particular for long wavelengths.

* Corresponding author. Tel.: +1 2547106873.
E-mail addresses: yang_li1@baylor.edu (Y. Li), mario.silveirinha@co.it.pt (M.G. Silveirinha).

http://dx.doi.org/10.1016/j.photonics.2014.06.002
1569-4410/

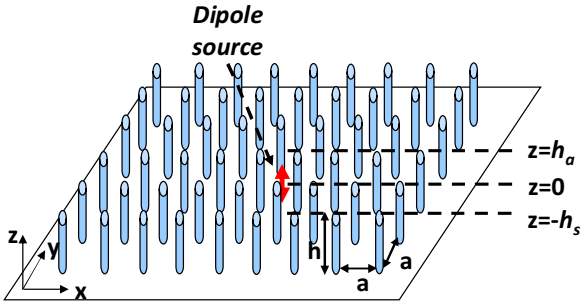

Fig. 1. A dielectric rod array setup.

Motivated by this application and with the aim to unveil the radiation and propagation mechanisms in a forest, here we investigate the radiation of an elementary short vertical dipole embedded within a metal-backed rod array from a theoretical viewpoint. The ground is supposed to model the electromagnetic response of the soil, and for simplicity here it is assumed to be a perfect electrical conductor (PEC). Our analysis is based on the effective medium model of metallic wire media developed in [22]. Analytical continuation arguments suggest that the same model may apply to ε-positive rod array as well. Using these ideas and techniques previously developed for metal wire arrays, we prove that the radiation fields can be expressed in the form of a Sommerfeld integral. Related problems were previously solved for perfectly conducting metal wire arrays [23,24]. Here we concentrate on dielectric rod arrays, aiming to understand the guided modes that are excited and the radiation mechanisms in this unique structure.

The article is organized as follows. In Section 2, the radiated fields are derived and written in the form of a Sommerfeld integral. In Section 3, the integral is evaluated numerically to generate near and far electric field data for both lossless and lossy dielectric rod arrays. The guided wave in the array is extracted and its propagation properties are highlighted. The results are compared with full-wave simulations. Section 4 summarizes our findings.

2. Theoretical model

Fig. 1 shows the geometry of the problem: a square array of dielectric rods is placed over a PEC ground plane. The rod height, rod radius, and the spacing between rods are h, r, and a, respectively. The source embedded inside the array is a vertical Hertzian dipole described by the current density $\vec{J}$ ($\vec{J} = j\omega p_e \delta(x, y, z)\hat{z}$, where p_e represents the electric dipole moment), and is placed at the height h_s above the PEC, and at a distance h_a below the air–slab interface. The permittivity of the rod and host medium are ε_m and ε_h, respectively, and the upper region is air.

Similar to the analysis of [23], first we define an intermediate normalized potential function Φ (which simply relates to the well-known magnetic vector potential A_z as $A_z = j\omega\mu_o p_e \Phi$), such that the electric field $\vec{E}$ in all space can be expressed as:

$$\frac{\vec{E}}{p_e} = \omega^2 \mu_o \Phi \hat{z} + \nabla\left(\frac{1}{\varepsilon_h(z)}\frac{\partial \Phi}{\partial z}\right) \tag{1}$$

The potential function Φ can be computed from its spectral domain counterpart $\tilde{\Phi}$. In [24], $\tilde{\Phi}$ for an unbounded dielectric rod array medium (formed by infinitely long dielectric wires) was found to be,

$$\tilde{\Phi} = \frac{1}{2\gamma_{qT}} C_{qT} e^{-\gamma_{qT}|z|} + \frac{1}{2\gamma_{TM}} C_{TM} e^{-\gamma_{TM}|z|} \tag{2}$$

where:

$$C_{qT} = \frac{\gamma_h^2 - \gamma_{TM}^2 + k_p^2}{\gamma_{qT}^2 - \gamma_{TM}^2} \tag{3.a}$$

$$C_{TM} = \frac{\gamma_h^2 - \gamma_{qT}^2 + k_p^2}{\gamma_{TM}^2 - \gamma_{qT}^2} \tag{3.b}$$

$$\gamma_{qT} = j\left[k_h^2 - \frac{1}{2}\left(k_p^2 + k_{||}^2 - \beta_c^2 - \sqrt{\left(k_p^2 + k_{||}^2 - \beta_c^2\right)^2 + 4k_{||}^2\beta_c^2}\right)\right]^{1/2} \tag{4.a}$$

$$\gamma_{TM} = j\left[k_h^2 - \frac{1}{2}\left(k_p^2 + k_{||}^2 - \beta_c^2 + \sqrt{\left(k_p^2 + k_{||}^2 - \beta_c^2\right)^2 + 4k_{||}^2\beta_c^2}\right)\right]^{1/2} \tag{4.b}$$

γ_{qT} and γ_{TM} are propagation constants for the quasi-TEM mode and TM mode in the dielectric rod array, respectively, k_p is the plasma wave number defined as $k_p = \sqrt{(2\pi/a^2)/\ln[a^2/4r(a-r)]}$, $k_h = \omega\sqrt{\mu_o\varepsilon_h}$, $k_{||} = \sqrt{k_x^2 + k_y^2}$, $\gamma_h = \sqrt{k_{||}^2 - k_h^2}$ and $\beta_c^2 = -\frac{k_p^2}{f_v}\frac{1}{\varepsilon_m/\varepsilon_h - 1}$.

Next we derive $\tilde{\Phi}$ for the dielectric rod array slab problem of Fig. 1 by making the following observations: (i) By the method of images, the PEC ground plane can be removed and a second vertical dipole can be placed $z = -2h_s$ without affecting the radiated fields above the ground plane; (ii) $\tilde{\Phi}$ must be an even function of $\bar{z}$ ($\bar{z} = z + h_s$) because of the symmetry of the problem; this property ensures that the tangential electric field is zero at the ground plane. Combining these observations with Eq. (2), we propose the following $\tilde{\Phi}$ for the dielectric rod array, which is an even function of $\bar{z}$:

$$\tilde{\Phi} = \frac{1}{2\gamma_{qT}}C_{qT}\left[e^{-\gamma_{qT}|z|} + e^{-\gamma_{qT}|z+2h_s|}\right] + \frac{1}{2\gamma_{TM}}C_{TM}\left[e^{-\gamma_{TM}|z|} + e^{-\gamma_{TM}|z+2h_s|}\right] + \quad -h_s < z < h_a \tag{5.a}$$
$$+A_{qT}\cosh\gamma_{qT}(z+h_s) + A_{TM}\cosh\gamma_{TM}(z+h_s)$$

$$\tilde{\Phi} = Te^{-\gamma_0(z-h_a)} \quad z > h_a \tag{5.b}$$

where $\gamma_0 = \sqrt{k_{||}^2 - k_0^2}$, and A_{qT}, A_{TM} and T are unknown coefficients which can be determined by imposing the following boundary conditions at the slab-air interface $z = h_a$:

(i) The continuity of the tangential components of the magnetic field at the interface requires that $\tilde{\Phi}$ is continuous. Hence,

$$\frac{1}{\gamma_{TM}}Q_{TM} + \frac{1}{\gamma_{qT}}Q_{qT} + A_{qT}\cosh(\gamma_{qT}h) + A_{TM}\cosh(\gamma_{TM}h) = T \tag{6.a}$$

where $Q_{TM} = \frac{1}{2}C_{TM}(e^{-\gamma_{TM}h_a} + e^{-\gamma_{TM}|h_a+2h_s|})$ and $Q_{qT} = \frac{1}{2}C_{qT}(e^{-\gamma_{qT}h_a} + e^{-\gamma_{qT}|h_a+2h_s|})$.

(ii) The continuity of the tangential components of the electric field at the interface requires that $1/\varepsilon_h(z)\,\partial\Phi/\partial z$ is continuous. Therefore,

$$Q_{TM} + Q_{qT} - A_{qT}\gamma_{qT}\sin h(\gamma_{qT}h) - A_{TM}\gamma_{TM}\sin h(\gamma_{TM}h) = \frac{\varepsilon_h}{\varepsilon_0}\gamma_0 T \tag{6.b}$$

(iii) Finally, for thin rods the microscopic polarization current at the ends of the rods should be negligible. Hence, similar to the wire medium case [25], one needs to use the additional boundary condition (ABC) that imposes that $k_h^2\Phi + \frac{\partial^2\Phi}{\partial z^2}$ is continuous at the interface, such that:

$$\gamma_{TM}Q_{TM} + \gamma_{qT}Q_{qT} + A_{qT}\gamma_{qT}^2\cosh(\gamma_{qT}h) + A_{TM}\gamma_{TM}^2\cos h(\gamma_{TM}h) = (\gamma_0^2 + k_0^2 - k_h^2)T \tag{6.c}$$

By solving the linear system Eq. (6.a)–(6.c) we found that the unknown coefficients are:

$$A_{qT} = \frac{Q_{TM}\left(\gamma_h^2 - \gamma_{TM}^2\right)(\cosh\gamma_{TM}h + \sinh\gamma_{TM}h)}{\gamma_{qT}\left(\gamma_h^2 - \gamma_{TM}^2\right)\cosh\gamma_{TM}h\sinh\gamma_{qT}h + \cosh\gamma_{qT}h\left[\frac{\varepsilon_h}{\varepsilon_0}\gamma_0\left(\gamma_{qT}^2 - \gamma_{TM}^2\right)\cosh\gamma_{TM}h + \gamma_{TM}\left(\gamma_{qT}^2 - \gamma_h^2\right)\sinh\gamma_{TM}h\right]} + \tag{7.a}$$
$$Q_{qT}\frac{-\left[\left(\gamma_h^2 - \gamma_{TM}^2\right) + \frac{\varepsilon_h}{\varepsilon_0}\frac{\gamma_0}{\gamma_{qT}}\left(\gamma_{TM}^2 - \gamma_{qT}^2\right)\right]\cosh\gamma_{TM}h - \frac{\gamma_{TM}}{\gamma_{qT}}\left(\gamma_h^2 - \gamma_{qT}^2\right)\sinh\gamma_{TM}h}{\gamma_{TM}\left(\gamma_h^2 - \gamma_{qT}^2\right)\cosh\gamma_{qT}h\sinh\gamma_{TM}h + \cosh\gamma_{TM}h\left[\frac{\varepsilon_h}{\varepsilon_0}\gamma_0\left(\gamma_{TM}^2 - \gamma_{qT}^2\right)\cosh\gamma_{qT}h + \gamma_{qT}\left(\gamma_{TM}^2 - \gamma_h^2\right)\sinh\gamma_{qT}h\right]}$$

$$A_{TM} = Q_{TM}\frac{-\left[\left(\gamma_h^2-\gamma_{qT}^2\right)+\frac{\varepsilon_h}{\varepsilon_0}\frac{\gamma_0}{\gamma_{TM}}\left(\gamma_{qT}^2-\gamma_{TM}^2\right)\right]\cosh\gamma_{qT}h-\frac{\gamma_{qT}}{\gamma_{TM}}\left(\gamma_h^2-\gamma_{TM}^2\right)\sinh\gamma_{qT}h}{\gamma_{qT}\left(\gamma_h^2-\gamma_{TM}^2\right)\cosh\gamma_{TM}h\sinh\gamma_{qT}h+\cosh\gamma_{qT}h\left[\frac{\varepsilon_h}{\varepsilon_0}\gamma_0\left(\gamma_{qT}^2-\gamma_{TM}^2\right)\cosh\gamma_{TM}h+\gamma_{TM}\left(\gamma_{qT}^2-\gamma_h^2\right)\sinh\gamma_{TM}h\right]}+$$
$$\frac{Q_{qT}\left(\gamma_h^2-\gamma_{qT}^2\right)\left(\cosh\gamma_{qT}h+\sinh\gamma_{qT}h\right)}{\gamma_{TM}\left(\gamma_h^2-\gamma_{qT}^2\right)\cosh\gamma_{qT}h\sinh\gamma_{TM}h+\cosh\gamma_{TM}h\left[\frac{\varepsilon_h}{\varepsilon_0}\gamma_0\left(\gamma_{TM}^2-\gamma_{qT}^2\right)\cosh\gamma_{qT}h+\gamma_{qT}\left(\gamma_{TM}^2-\gamma_h^2\right)\sinh\gamma_{qT}h\right]} \tag{7.b}$$

$$T = \frac{Q_{TM}\left(\gamma_{qT}^2-\gamma_{TM}^2\right)\cosh\gamma_{qT}h\left(\cosh\gamma_{TM}h+\sinh\gamma_{TM}h\right)}{\gamma_{qT}\left(\gamma_h^2-\gamma_{TM}^2\right)\cosh\gamma_{TM}h\sinh\gamma_{qT}h+\cosh\gamma_{qT}h\left[\frac{\varepsilon_h}{\varepsilon_0}\gamma_0\left(\gamma_{qT}^2-\gamma_{TM}^2\right)\cosh\gamma_{TM}h+\gamma_{TM}\left(\gamma_{qT}^2-\gamma_h^2\right)\sinh\gamma_{TM}h\right]}+$$
$$\frac{Q_{qT}\left(\gamma_{TM}^2-\gamma_{qT}^2\right)\cosh\gamma_{TM}h\left(\cosh\gamma_{qT}h+\sinh\gamma_{qT}h\right)}{\gamma_{TM}\left(\gamma_h^2-\gamma_{qT}^2\right)\cosh\gamma_{qT}h\sinh\gamma_{TM}h+\cosh\gamma_{TM}h\left[\frac{\varepsilon_h}{\varepsilon_0}\gamma_0\left(\gamma_{TM}^2-\gamma_{qT}^2\right)\cosh\gamma_{qT}h+\gamma_{qT}\left(\gamma_{TM}^2-\gamma_h^2\right)\sinh\gamma_{qT}h\right]} \tag{7.c}$$

This enables us to write $\tilde{\Phi}$ in a closed-analytical form. The normalized potential function Φ is computed by the taking the inverse Fourier transform (see [23,24]):

$$\Phi = \frac{1}{2\pi}\int_0^{+\infty}\tilde{\Phi}J_0\left(k_{||}\rho\right)k_{||}dk_{||} \tag{8}$$

where $\rho=\sqrt{x^2+y^2}$ and J_0 is the first kind Bessel function. By numerically calculating this Sommerfeld-type integral it is possible to characterize both the near and far radiated fields.

3. Near and far fields

In the first example, we study the dipole emission in a lossless dielectric rod array. Each rod of the array has permittivity $\varepsilon_m = 81\varepsilon_0$ (ε_0 is the free space permittivity), radius $r = 3.8$ mm, and height $h = 20.5$ cm. The spacing a between rods is 6 cm. The array size at 1 GHz is approximately equal to a 1:50 scaling of forest at 20 MHz. The dipole is placed at the ground plane level ($h_s = 0$). For each frequency, the radiated near electric fields are computed at different distances x and different height z away from the source. To avoid singularities in the Sommerfeld integral, the integration path is detoured in the upper half of the complex $k_{(||)}$ plane.

Fig. 2(a) and (b) depicts the near electric fields at 1 GHz calculated with the analytical model. The horizontal distance x ranges from 0 to 1.8 m and the height z extends from 0 to 0.6 m. The color represents the normalized E_z and E_x field strength on a dB scale. It is seen that both components are very intense inside the rod array, and decay slowly along the x axis due to the absence of loss. For comparison, Fig. 2(c) and (d) shows the same fields calculated with a full-wave simulation. The array size is finite (6×36) in the full-wave simulations, and this leads to strong reflections from the end of array and to an interference pattern. To make a more quantitative comparison between theory and simulation, the normalized E_z and E_y at height $z = 9$ cm are plotted against x in Fig. 2(e) and (f). We can see that the theory and simulation results are qualitatively similar to each other. The differences can be attributed to the array size (infinite in theory vs. finite in simulation) and to the reflections from the array boundaries.

To better understand the radiation mechanisms, we characterized the guided modes of the rod array substrate. The characteristic equation of for the guided modes corresponds to the pole of the Sommerfeld integrand, that is:

$$\left\{\gamma_{TM}(\gamma_h^2-\gamma_{qT}^2)\tanh(\gamma_{TM}h)+\left[\frac{\varepsilon_h}{\varepsilon_0}\gamma_0(\gamma_{TM}^2-\gamma_{qT}^2)+\gamma_{qT}(\gamma_{TM}^2-\gamma_h^2)\tanh(\gamma_{qT}h)\right]\right\}\times$$
$$\left\{\gamma_{qT}(\gamma_h^2-\gamma_{TM}^2)\tanh(\gamma_{qT}h)+\left[\frac{\varepsilon_h}{\varepsilon_0}\gamma_o(\gamma_{qT}^2-\gamma_{TM}^2)+\gamma_{TM}(\gamma_{qT}^2-\gamma_h^2)\tanh(\gamma_{TM}h)\right]\right\}=0 \tag{9}$$

By solving this characteristic equation it is found that there is a propagating guided mode that is a slow wave below 1.3 GHz. Fig. 3 shows the normalized propagation constants of this guided mode versus frequency. The modal field distribution of this guided mode at 1 GHz is plotted in Fig. 4 against the height z. For comparison, the mode propagation

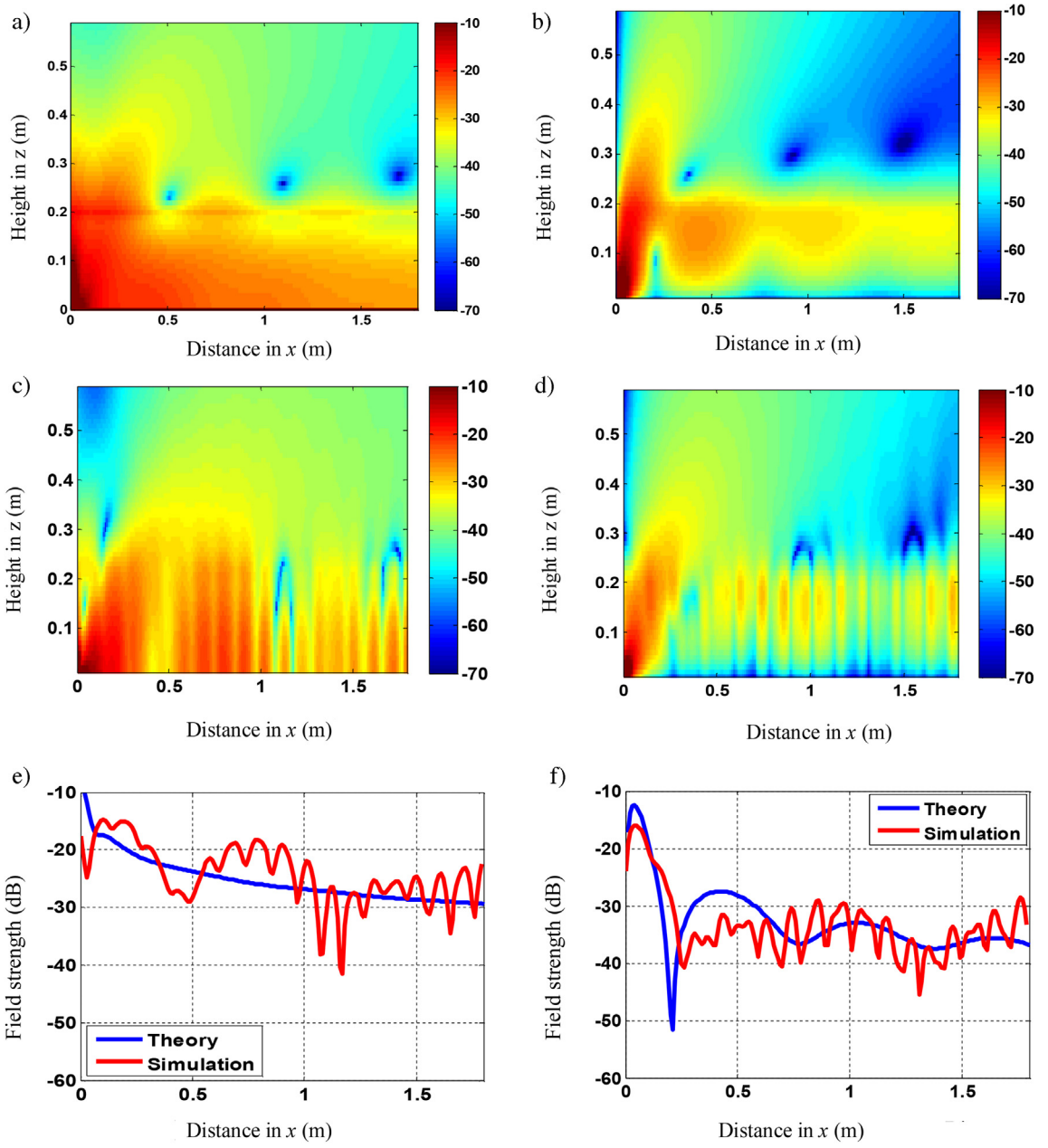

Fig. 2. Near electric fields in the dielectric rod array ($\varepsilon_m = 81\,\varepsilon_o$) at 1 GHz: (a) E_z theory (infinite array), (b) E_x theory (infinite array), (c) E_z full wave simulation (truncated array), (d) E_x full wave simulation (truncated array), (e) amplitude of E_z at $z = 9$ cm, (f) amplitude of E_x at $z = 9$ cm.

constant and field distribution are also extracted from the full-wave simulation data using the ESPRIT algorithm [26]. The simulation results ($k_{||\_simulation} = 1.491\,k_o$ at 1 GHz and the simulated field height profile in Fig. 4) show excellent agreement with the theory predictions. The excitation of this mode explains why the radiated field decays relatively slowly along the x-direction.

We also investigated the dipole radiation in a lossy dielectric rod array. The array geometrical parameters are the same as in the previous example, but the permittivity of rods is altered to $\varepsilon_m = (81\text{-}j20)\varepsilon_o$. Fig. 5 (a) and (b) shows the normalized E_z and E_x in the lossy array at 1 GHz. Full wave simulation results are shown in Fig. 5 (c) and (d). Compared

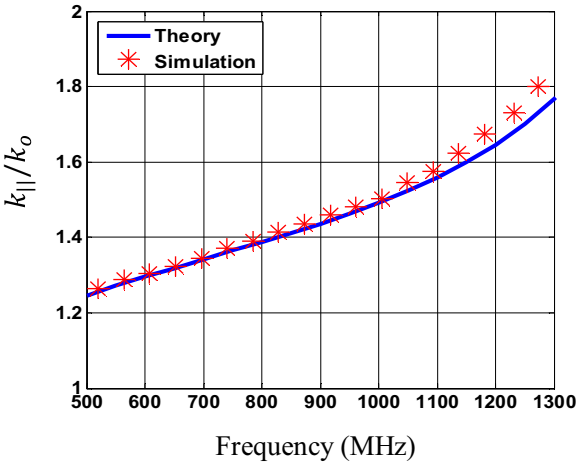

Fig. 3. Normalized propagation constants of the guided mode in the rod array ($\varepsilon_m = 81\,\varepsilon_o$).

to the lossless case [Fig. 2], the field strengths in the lossy array are much weaker and decay faster. Fig. 5 (e) and (f) depict the E_z and E_x field strengths at $z = 9$ cm in the lossy array. They show reasonable agreement. The E_z component is more affected by the material absorption since it experiences stronger scatterings from the vertically-oriented rods, and thus its strength is more dependent upon the number of rods in the array.

The propagation constant of the guided wave in the lossy array is found to be $(1.482\text{-}j0.157)k_o$ from theory and $(1.481\text{-}j0.155)k_o$ from simulation at 1 GHz. Fig. 6 (a) and (b) exhibits the modal field distribution from both theory and simulation. Good agreement is obtained and the modal profiles are analogous to those of the lossless array [Fig. 4].

We also computed the propagation characteristics of the guided mode versus rod spacing in the lossy rod array at 1 GHz. In Fig. 7(a), it can be seen that the propagation constants of the guided mode increase as the spacing between rods decreases (i.e., as the rod density increases and the periodic array becomes more and more similar to a continuous dielectric slab), implying that a higher effective dielectric constant is reached for a denser array. A similar trend can be observed in Fig. 7(b) for the attenuation constant, implying higher propagation loss in a dense, lossy dielectric rod array.

To separate the guided mode (surface wave) and the space wave contributions, we have computed the guided wave residue at its pole at 1 GHz for both the lossless and lossy dielectric rod arrays, and compared the result with the radiation field obtained with the deformed path integration. The residue calculation results are shown in the Fig. 8 below. It is seen that the guided wave pole contribution (Fig. 8 (a)) shows good agreement with the deformed path

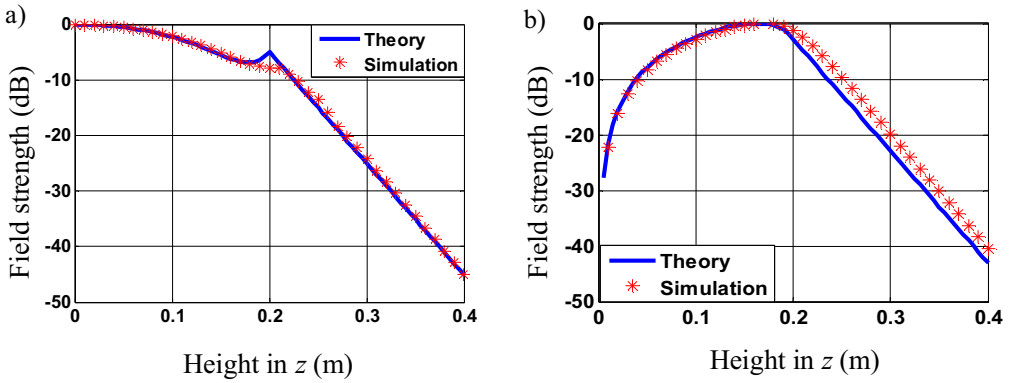

Fig. 4. Extracted height profiles of the guided mode at 1 GHz in the rod array ($\varepsilon_m = 81\,\varepsilon_o$): (a) E_z, (b) E_x.

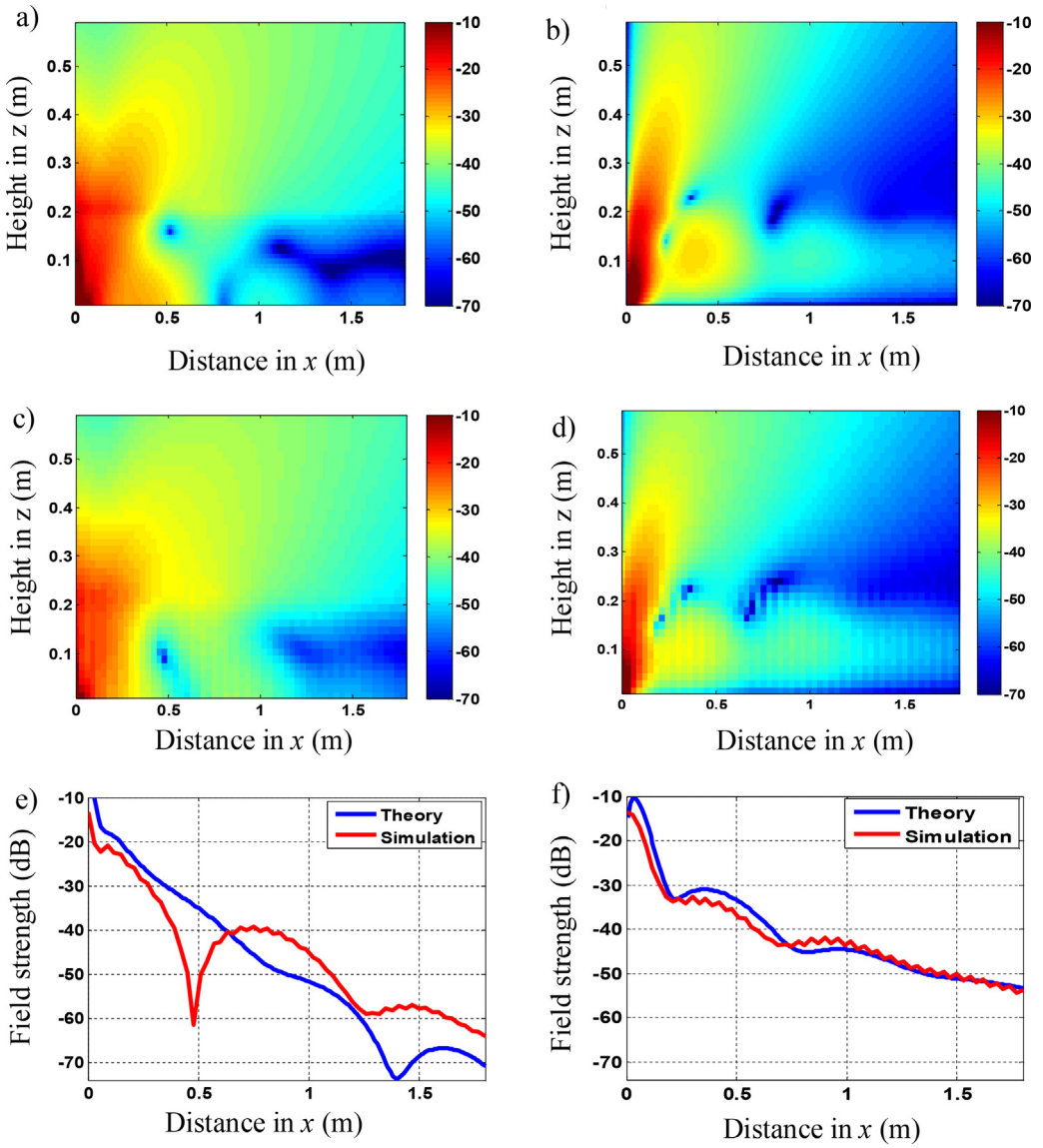

Fig. 5. Near electric fields in the lossy dielectric rod array at 1 GHz ($\varepsilon_m = (81\text{-}j20)\varepsilon_o$): (a) E_z theory (infinite array), (b) E_x theory (infinite array), (c) E_z full wave simulation (truncated array), (d) E_x full wave simulation (truncated array), (e) amplitude of E_z at $z = 9$ cm, (f) amplitude of E_x at $z = 9$ cm.

integration result (Fig. 2 (a)) inside the lossless dielectric rod array. The differences for the lossy dielectric rod array can be attributed to the space wave contribution (Fig. 8 (b) vs. Fig. 5 (a)).

Finally, we compute the dipole radiated far fields for both lossless and lossy dielectric rod arrays. Fig. 9(a) and (b) depicts the normalized far field patterns in the elevation plane ($\phi = 90^\circ$) at 0.75 GHz, 1 GHz and 1.25 GHz. We also compute the radiation patterns in the infinite size array using full-wave simulation tool FEKO and the reciprocity theorem [27]. The simulation results agree well with the theory predictions, and both indicate main beam directions of $\theta = 62.75^\circ$ for $\varepsilon_m = 81\varepsilon_o$ array and $\theta = 67.5^\circ$ for $\varepsilon_m = (81\text{-}j20)\,\varepsilon_o$ array at 1 GHz. It is well-known that the main beam angle is equal to $\theta = 90^\circ$ for the dipole radiation in the free space. Hence, as compared to the free-space situation, the main beam shifts away from the end-fire direction. We also verified (not shown here) that the radiation pattern is not significantly disturbed with changes in the period a. This finding may provide insights for study of antenna radiation in a forest environment.

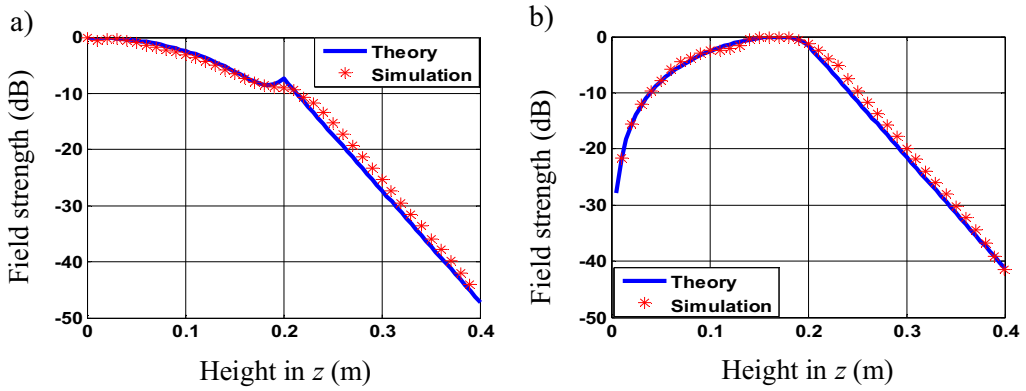

Fig. 6. Extracted height profiles of the guided mode in the lossy rod array ($\varepsilon_m = (81\text{-}j20)\varepsilon_o$): (a) E_z, (b) E_x.

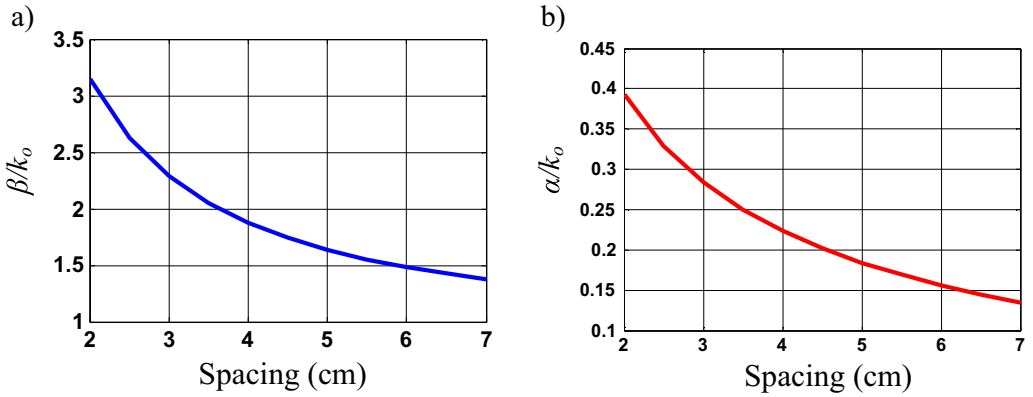

Fig. 7. Extracted guided mode propagation characteristics for the lossy ($\varepsilon = (81\text{-}j20)\varepsilon_o$) rod arrays at different rod spacings at 1 GHz: (a) normalized propagation constants. (b) Normalized attenuation constants.

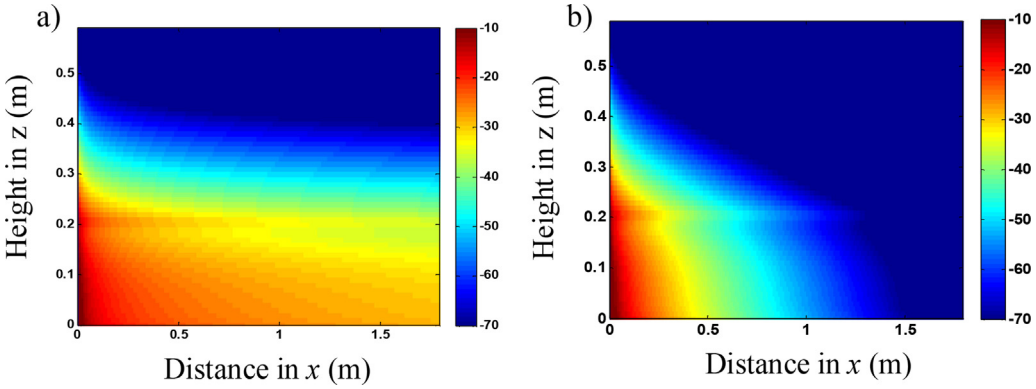

Fig. 8. Computed residue contributions at the guided mode poles at 1 GHz: (a) lossless rod array (b) Lossy rod array.

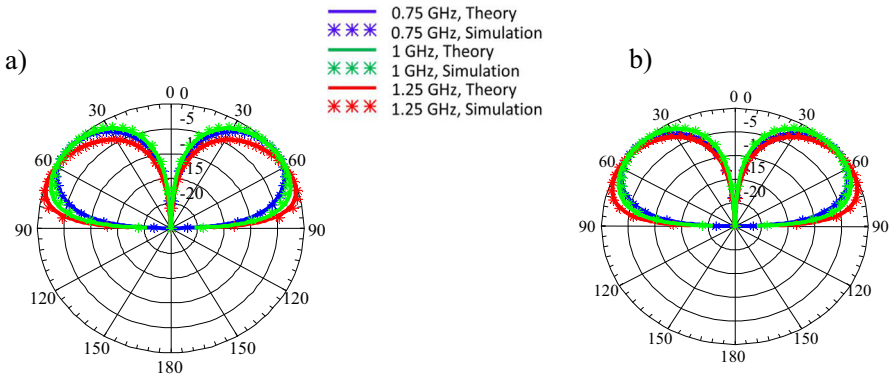

Fig. 9. Far field patterns in the elevation plane (on dB scale) at 0.75 GHz, 1 GHz and 1.25 GHz (a) $\varepsilon_m = 81\varepsilon_o$ array, (b) $\varepsilon_m = (81\text{-}j20)\varepsilon_o$ array.

4. Conclusions

In this paper, we obtained the field radiated by a short dipole embedded in a metal-backed rod array based on an analytical effective medium model that reduces the problem to the calculation of a Sommerfeld-type integral. Using this theory we computed the near and far fields of lossless and lossy arrays. It was found that both space and surface (guided) waves can be excited. The modal fields and propagation constants of the guided modes were found to compare very well with full-wave simulations. On the other hand, the far-field exhibits a radiation intensity maximum away from the end-fire direction.

It should be pointed out the proposed effective medium model only applies to a rod array with rod radius much smaller than both the height and the wavelength. This "thin-wire" assumption is required since the transverse polarization of the rod has been neglected in the derivation [24]. Moreover, the spacing between rods should be considerably smaller than a wavelength as well, so that the rod array can be homogenized as an effective medium.

For future study, we are currently exploring the possibility of randomizing the dielectric rod array, and substituting the PEC ground plane by a more realistic lossy dielectric ground, such that the new structure can serve as a better model for forest propagation study.

Acknowledgment

The authors wish to thank Prof. Ali Yilmaz from the University of Texas at Austin for providing the full-wave simulation data for comparison.

References

[1] L.R. Lewis, A. Hessel, G.H. Knittel, Performance of protruding-dielectric waveguide element in a phased array, IEEE Trans. Antennas Propagat. 20 (November) (1972) 712–722.
[2] S.G. Johnson, S. Fan, P.R. Villeneuve, J.D. Joannopoulos, Guided modes in photonic crystal slabs, Phys. Rev. B 60 (1999) 5751–5758.
[3] J.B. Pendry, A.J. Holden, W.J. Stewart, I. Youngs, Extremely low frequency plasmons in metallic meso structures, Phys. Rev. Lett. 76 (1996) 4773–4776.
[4] S.I. Maslovski, S.A. Tretyakov, P.A. Belov, Wire media with negative effective permittivity: a quasi-static model, Microw. Opt. Technol. Lett. 35 (1) (2002) 47–51.
[5] P.A. Belov, R. Marqués, S.I. Maslovski, M. Silveirinha, C.R. Simovski, S.A. Tretyakov, Strong spatial dispersion in wire media in the very large wavelength limit, Phys. Rev. B 67 (2003) 113103-1–113103-4.
[6] P.A. Belov, Y. Hao, S. Sudhakaran, Subwavelength microwave imaging using an array of parallel conducting wires as a lens, Phys. Rev. B 73 (1–4) (2006) 033108.
[7] M.G. Silveirinha, P.A. Belov, C. Simovski, Subwavelength imaging at infrared frequencies using an array of metallic nanorods, Phys. Rev. B 75 (1–12) (2007) 035108.
[8] C.R. Simovski, P.A. Belov, A.V. Atrashchenko, Yu.S. Kivshar, Wire metamaterials: physics and applications, Adv. Mater. 24 (31) (2012) 4229–4248.
[9] T. Schibli, K. Minoshima, H. Kataura, E. Itoga, N. Minami, S. Kazaoui, K. Miyashita, M. Tokumoto, Y. Sakakibara, Ultrashort pulsegeneration by saturable absorber mirrors based on polymer-embedded carbon nanotubes, Opt. Express 13 (2005) 8025–8031.

[10] S.I. Maslovski, M.G. Silveirinha, Ultralong-range Casimir–Lifshitz forces mediated by nanowire materials, Phys. Rev. A 82 (2) (2010) 022511.
[11] D.E. Fernandes, S.I. Maslovski, M.G. Silveirinha, Cherenkov emission in a nanowire material, Phys. Rev. B 85 (15) (2012) 155107.
[12] A.V. Tyukhtin, V.V. Vorobev, Cherenkov radiation in a metamaterial comprised of coated wires, J. Opt. Soc. Am. B 30 (2013) 1524–1531.
[13] V.V. Vorobev, A.V. Tyukhtin, Nondivergent Cherenkov radiation in a wire metamaterial, Phys. Rev. Lett. 108 (2012) 184801.
[14] S.M. Hashemi, I.S. Nefedov, Wideband perfect absorption in arrays of tilted carbon nanotubes, Phys. Rev. B 86 (19) (2012) 195411.
[15] A.N. Poddubny, P.A. Belov, Y.S. Kivshar, Purcell effect in wire metamaterials, Phys. Rev. B 87 (3) (2013) 035136.
[16] C.A. Valagiannopoulos, I.S. Nefedov, Increasing the electromagnetic attenuation below a quasi-matched surface with use of passive hyperbolic metamaterials, Photon. Nanostruct. Fundam. Appl. 11 (August) (2013) 182–190.
[17] I.S. Nefedov, C.A. Valagiannopoulos, S.M. Hashemi, E.I. Nefedov, Total absorption in asymmetric hyperbolic media, Sci. Rep. 3 (2013) 2662, http://dx.doi.org/10.1038/srep02662.
[18] C.R. Simovsky, S. Maslovski, I. Nefedov, A. Tretyakov, Optimization of radiative heat transfer in hyperbolic metamaterials for thermophotovoltaic applications, Opt. Express 21 (2013) 14988.
[19] G.I. Torgovnikov, Dielectric Properties of Wood and Wood-Based Materials, Springer-Verlag, NY, 1993.
[20] Y. Li, H. Ling, Investigation of wave propagation in a dielectric rod array: towards the understanding of HF/VHF propagation in a forest, IEEE Trans. Antennas Propagat. 58 (December) (2010) 4025–4032.
[21] Y. Li, M.F. Wu, A. Yilmaz, H. Ling, On wave propagation mechanisms in a dielectric rod array, IEEE Trans. Antennas Propagat. 61 (April) (2013) 2337–2342.
[22] M.G. Silveirinha, Nonlocal homogenization model for a periodic array of epsilon-negative rods, Phys. Rev. E 73 (2006) 046612.
[23] Y. Li, M.G. Silveirinha, Radiation from a Hertzian dipole embedded in a wire-medium slab, IEEE Antennas Wireless Propagat. Lett. 12 (2013) 401–404.
[24] M.G. Silveirinha, S.I. Maslovski, Radiation from elementary sources in a uniaxial wire medium, Phys. Rev. B 85 (2012) 155125.
[25] M.G. Silveirinha, Additional boundary condition for the wire medium, IEEE Trans. Antennas Propagat. 54 (June) (2006) 1766–1780.
[26] Y. Li, H. Ling, Extraction of wave propagation mechanisms in a cut-wire array using the ESPRIT algorithm, IEEE Antennas Wireless Propagat. Lett. 8 (2009) 744–747.
[27] K.P.B. Burghignoli, G. Lovat, F. Capolino, D.R. Jackson, D.R. Wilton, Directive leaky-wave radiation from a dipole source in a wire-medium slab, IEEE Trans. Antennas Propagat. 56 (May) (2008) 1329–1339.